*mathematics*

MDPI

*Article*

# Approximations for Secular Variation Maxima of Classical Orbital Elements under Low Thrust

**Zhaowei Wang [1], Lin Cheng [2] and Fanghua Jiang [1,*]**

[1] School of Aerospace Engineering, Tsinghua University, Beijing 100084, China
[2] School of Astronautics, Beihang University, Beijing 100083, China
* Correspondence: jiangfh@tsinghua.edu.cn; Tel.: +86-010-6279-4365

**Abstract:** The reachability assessment of low-thrust spacecraft is of great significance for orbital transfer, because it can give a priori criteria for the challenging low-thrust trajectory design and optimization. This paper proposes an approximation method to obtain the variation maximum of each orbital element. Specifically, two steps organize the contribution of this study. First, combined with functional approximations, a set of analytical expressions for the variation maxima of orbital elements over one orbital revolution are derived. Second, the secular approximations for the variation maxima of the inclination and the right ascension of the ascending node are derived and expressed explicitly. An iterative algorithm is given to obtain the secular variation maxima of the other orbital elements the orbital elements other than the inclination and right ascension of the ascending node. Numerical simulations for approximating the variation maxima and a preliminary application in estimation of the velocity increment are given to demonstrate the efficiency and accuracy of the proposed method. Compared with the indirect method used alone for low-thrust trajectory optimization, the computation burden of the proposed method is reduced by over five orders of magnitude, and the computational accuracy is still high.

**Keywords:** low-thrust orbital transfer; trajectory optimization; variations of orbital elements; reachability assessment; estimation of velocity increment

**MSC:** 70M20



**Citation:** Wang, Z.; Cheng, L.; Jiang, F. Approximations for Secular Variation Maxima of Classical Orbital Elements under Low Thrust. *Mathematics* **2023**, *11*, 744. https://doi.org/10.3390/math11030744

Academic Editors: Yu Jiang and Haijun Peng

Received: 1 January 2023
Revised: 24 January 2023
Accepted: 26 January 2023
Published: 2 February 2023



## 1. Introduction

Interplanetary space missions propelled by solar electric propulsion, such as the Deep Space 1 [1] and BepiColombo [2], have demonstrated that low-thrust propulsion can be an alternative propulsion other than the traditional chemical propulsion for space exploration missions. Benefiting from its high propellant efficiency, this low-thrust electric propulsion system is drawing increasing attention from researchers. Space missions propelled by the low-thrust propulsion system are increasing rapidly [3,4]. Assessment of the state reachability of the low-thrust spacecraft provides meaningful reference for the preliminary design of space missions, such as multitarget missions [3,5], multiple debris removal missions [6], and collision avoidance missions [7–9]. It enables us to develop a smarter autonomous spacecraft [10]. Existing studies mainly focus on the reachability of impulsive spacecraft, while there are few studies on the reachability of low-thrust spacecraft. Therefore, this paper aims to develop a methodology that assesses the reachability of low-thrust orbital transfers. It should be able to benefit the global trajectory optimization for multitarget missions.

Numerous researchers focus on the reachability of spacecraft propelled with impulsive thrust [11–17]. For example, the upper bound [12] for the reachable domain was determined for spacecraft with a single fixed-magnitude impulse. Vinh et al. [15] analyzed the reachable surface of an interceptor at a given time. Otherwise, the reachability was also analyzed for spacecraft with a given impulse in a definite direction, such as a tangent impulse [16] and a

norm impulse [17]. These studies have given wide analyses of the reachability of spacecraft with different impulses.

The reachability assessment of the low-thrust spacecraft can be obtained by solving for the variation ranges of orbital elements. The variation extrema of orbital elements can be modeled as optimal control problems [18]. The indirect methods and direct methods [19], specifically, such as the primer vector theory [20,21] and the convex optimization [22], are usually applied to solving the optimal control problems. However, the initial guesses of the shooting unknowns and multiple shooting strategies are usually needed by the indirect and direct methods. Moreover, the equations of the motion of the spacecraft propelled by the low thrust is generally non-integrable. Thus, numerical propagation of the low-thrust trajectories is fundamental but time-consuming when used to solve the trajectory optimization problems [19,23–25]. To improve the solution efficiency, two major ways have been developed. The first way is to simplify the motion equation. For example, the Fourier series expansions were applied to approximate the thrust profiles [26–28] and the equations of motion [29–31]. However, a nonlinear programming solver was needed to generate an approximate optimal trajectory by optimizing the coefficients of the Fourier series. The second way is to predict the evolution of the orbital elements [32] of low-thrust spacecraft, specifically, such as the semi-analytical theory [33], the orbital averaging method [34], and the asymptotic solution for the orbital motion subjected to constant thrust [35,36]. With the short-periodic terms ignored, Gao et al. [34] have made significant efforts to find an analytical solution for the evolutions of the orbital elements considering the J2 perturbation and the Earth shadow. Recently, innovative artificial intelligence methods such as machine learning have been applied in orbital guidance and control [37–39]. However, the machine learning methods are now still suffering from unknown black-box optimization models. To some extent, these two ways, simplifying the equations of motion and predicting the orbital evolution, can improve the computational efficiency and convergence rate when used to solve the optimal control problems. However, these methods are still time-consuming because they still rely heavily on numerical methods.

In order to assess the reachability of a low-thrust transfer, an effective approximation is necessary to obtain the variation ranges of the classical orbital elements of low-thrust spacecraft propelled over a long period of time. The variation maximum of each orbital element will be investigated analytically in this paper, and their variation minima can be obtained in the same way, but is omitted here for the sake of conciseness. The contribution of this paper is accomplished in two steps. Firstly, combined with functional approximations, the variation maxima of classical orbital elements over one orbital revolution are derived analytically by applying the local optimal control profile. Secondly, a set of explicit expressions are derived and an iteration algorithm is established to obtain the approximation for the secular maximum of each orbital element. The simulation results will demonstrate the efficiency and accuracy of the proposed method over the indirect method.

The rest of this paper is organized as follows. In Section 2, Gauss's variational equations for classical orbital elements are listed, and several simplifying assumptions are stated. In Section 3, the analytical approximation to the secular variation maximum of each classical orbital element is proposed. The model for the indirect method used to solve the variation maxima of the orbital elements is expressed first in Section 4, and then the simulations for the approximations of the variation maxima and the estimation of the velocity increment are described. Finally, the conclusion is drawn in Section 6.

## 2. Gauss's Variational Equations and Simplifying Assumptions

Gauss's variational equations will be listed, where the thrust acceleration vector is projected onto the tangential-normal coordinate frame. Then, three assumptions will be stated, based on which Gauss's variational equations are simplified so that the secular variation maxima of the classical orbital elements can be investigated analytically.

### 2.1. Gauss's Variational Equations for Classical Orbital Elements

The Gauss's variational equations with respect to time $t$ in tangential-normal coordinates are expressed in the forms [11]

$$\frac{\mathrm{d}a}{\mathrm{d}t} = \frac{2a^2 v}{\mu} a_t \tag{1}$$

$$\frac{\mathrm{d}e}{\mathrm{d}t} = \frac{1}{v}\left[2(e+\cos f)a_t - \frac{r}{a}\sin f a_n\right] \tag{2}$$

$$\frac{\mathrm{d}i}{\mathrm{d}t} = \frac{r\cos\theta}{h} a_h \tag{3}$$

$$\frac{\mathrm{d}\Omega}{\mathrm{d}t} = \frac{r\sin\theta}{h\sin i} a_h \tag{4}$$

$$\frac{\mathrm{d}\omega}{\mathrm{d}t} = \frac{1}{ev}\left[2\sin f a_t + \left(2e + \frac{r}{a}\cos f\right)a_n\right] - \frac{r\sin\theta\cos i}{h\sin i} a_h \tag{5}$$

$$\frac{\mathrm{d}f}{\mathrm{d}t} = \frac{h}{r^2} - \frac{1}{ev}\left[2\sin f a_t + \left(2e + \frac{r}{a}\cos f\right)a_n\right] \tag{6}$$

where $\theta = \omega + f$ denotes the argument of latitude, $r = \frac{h^2}{\mu(1+e\cos f)}$ represents the orbital radius, and $v = \frac{\mu}{h}\sqrt{e^2+1+2e\cos f}$ represents the orbital velocity. The vector $\boldsymbol{a} = [a_t, a_n, a_h]$ denotes the propulsive acceleration vector projected onto the tangential-normal coordinate frame, which is shown in Figure 1. The unit vector $\boldsymbol{e_t}$ lies in the plane of the osculating orbit along the velocity vector, $\boldsymbol{e_h}$ is along the specific angular momentum vector, and $\boldsymbol{e_n}$ is towards the central body and forms the right-handed coordinate system with the other two components.

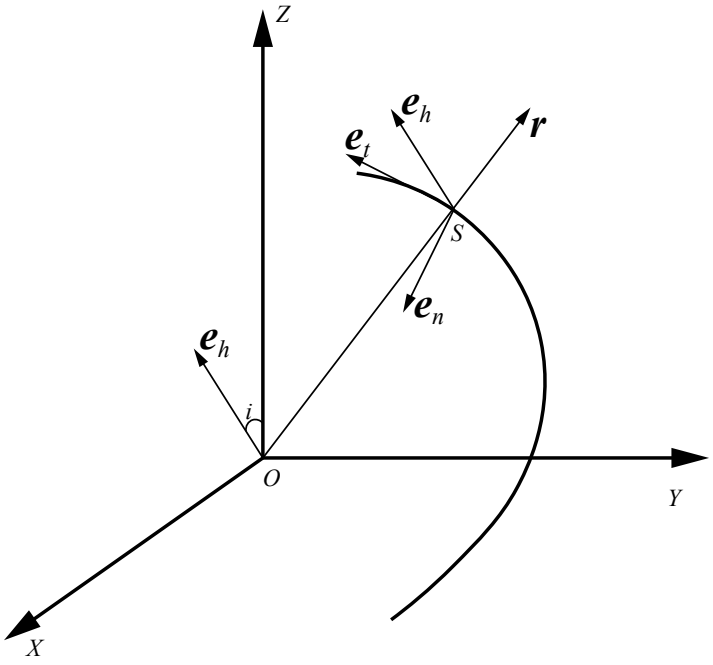


**Figure 1.** Tangential-normal coordinate frame.

### 2.2. Simplifying Assumptions

To approximate the secular variations of the classical orbital elements, some assumptions are needed to simplify the variational Equations (1)–(6). They are as follows

1. The fuel consumption is small and ignored due to the low magnitude of the thrust compared to the total mass of the spacecraft. Consequently, the magnitude of the propulsive acceleration $a_{\max}$ becomes constant because of the constant low-thrust magnitude $T_{\max}$. Thus, the following equation holds

$$\|\boldsymbol{a}\| = \frac{T_{\max}}{m} = a_{\max} = \text{const} \tag{7}$$

The thrust magnitude $T_{\max}$ is modeled as a function of the maximum thruster input power $P_{\max}$ and specific impulse $I_{\text{sp}}$ as [40]

$$T_{\max} = \frac{2\eta P_{\max}}{I_{\text{sp}} g_0} \tag{8}$$

where $\eta$ denotes the thruster efficiency, whose value together with $P_{\max}$ are selected from [40]. They are assumed to be constant in this paper to obtain a constant low-thrust magnitude. Meanwhile, $g_0 = 9.80665\,\text{m/s}^2$ is the standard gravitational acceleration.

2. The variation of the true anomaly caused by the three components of $\boldsymbol{a}$ can be ignored because its maximum $a_{\max}$ is much smaller than the central gravitational acceleration [34].

$$\frac{\mathrm{d}f}{\mathrm{d}t} \approx \frac{h}{r^2} \tag{9}$$

In Equation (9), the approximation of the Equation (6) can be derived when the effect on $\mathrm{d}f/\mathrm{d}t$ caused by the low thrust is small enough compared to the term $h/r^2$ (a similar approximation can also obtained in [36,41]).
Divided by Equation (9), Gauss's variational equations of classical orbital elements are transformed into the following differential equations in terms of the true anomaly

$$\frac{\mathrm{d}a}{\mathrm{d}f} = \frac{2a^2 r^2 v}{\mu h} a_t \tag{10}$$

$$\frac{\mathrm{d}e}{\mathrm{d}f} = \frac{r^2}{hv}\left[2(e+\cos f)a_t - \frac{r}{a}\sin f a_n\right] \tag{11}$$

$$\frac{\mathrm{d}i}{\mathrm{d}f} = \frac{r^3\cos\theta}{h^2} a_h \tag{12}$$

$$\frac{\mathrm{d}\Omega}{\mathrm{d}f} = \frac{r^3\sin\theta}{h^2\sin i} a_h \tag{13}$$

$$\frac{\mathrm{d}\omega}{\mathrm{d}f} = \frac{r^2}{hev}\left[2\sin f a_t + \left(2e + \frac{r}{a}\cos f\right)a_n\right] - \frac{r^3\sin\theta\cos i}{h^2\sin i} a_h \tag{14}$$

3. Owing to their very small variations within one revolution, the orbital elements are assumed to be unchanged within every orbital revolution when the related right sides of Equations (10)–(14) are used to estimate the variations of orbital elements immediately after the revolution.

## 3. Secular Variation Maximum of Single Classical Orbital Element

Based on the previous assumptions, the approximations for the secular variation maxima of the classical orbital elements are derived and expressed as some semi-analytical formulas in this section. First, we try to derive the approximation for the variation maximum of each orbital element over one orbital revolution analytically. Second, we focus only on the variations of the orbital elements immediately after integer revolutions but ignore the short-term variations within one orbital revolution.

The procedure for approximating the secular variation maxima of the classical orbital elements is shown in Figure 2.

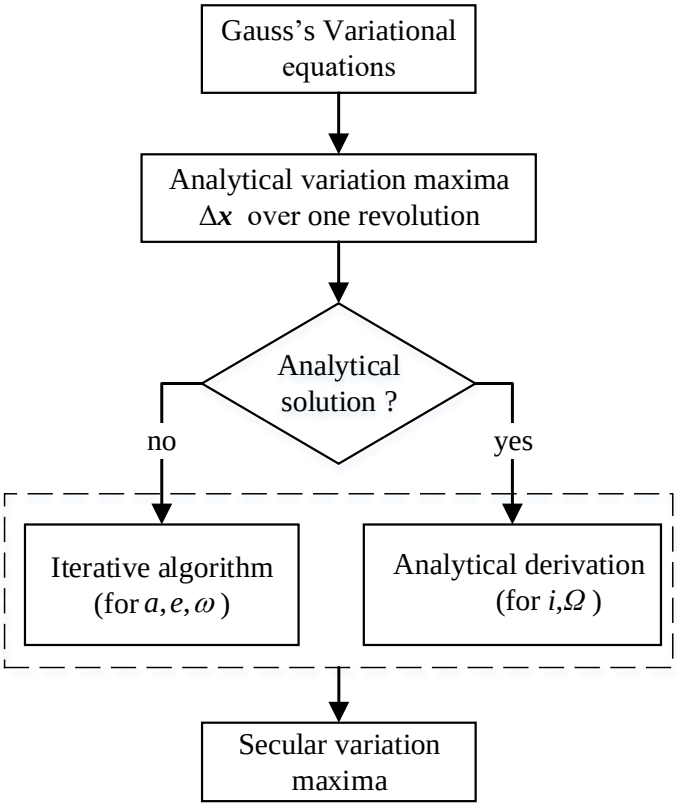


**Figure 2.** Procedure for approximating the secular variation maxima.

As shown in Figure 2, the secular variation maximum of each orbital element is obtained through two steps. The variation maximum over one orbital revolution, $\Delta \boldsymbol{x}$, is solved at first. Then, the approximations for the secular variation maxima of the orbital elements are divided into two groups. For the three orbital elements $a, e$, and $\omega$, an iterative algorithm is used to obtain their secular variation maxima. Meanwhile, two analytical solutions are derived to obtain those for $i$ and $\Omega$.

### *3.1. Secular Variation Maximum of Semi-Major Axis*

Replacing the orbital velocity in Equation (10) with its well-known expression with respect to the COE results in the semi-major axis with respect to the true anomaly:

$$\frac{\mathrm{d}a}{\mathrm{d}f} = \frac{2a_t a^3(1-e^2)}{\mu} \frac{\sqrt{1+e^2+2e\cos f}}{(1+e\cos f)^2} \tag{15}$$

which demonstrates that the well-known way to maximize the variation of the semi-major axis is to apply the acceleration along the tangent direction.

When the orbital elements remain unchanged within one revolution, as assumed in Section 2.2, the variation maximum of the semi-major axis over one revolution, denoted by $\Delta a_N$, is derived

$$\Delta a_N = \frac{2a_{N-1}^3(1-e_{N-1}^2)a_t}{\mu} C_{I,N-1} \tag{16}$$

where the parameter $C_{I,N-1}$ expressed by the definite integral (17) remains unchanged, as the eccentricity $e_{N-1}$ remains unchanged within the $(N-1)$-th orbital revolution.

$$\begin{aligned} C_{I,N-1} &= \int_0^{2\pi} \frac{\sqrt{1+e_{N-1}^2+2e_{N-1}\cos f}}{(1+e_{N-1}\cos f)^2}\mathrm{d}f \\ &= \frac{4\mathrm{EllipticE}(e_{N-1})}{1-e_{N-1}^2} \end{aligned} \tag{17}$$

where $\mathrm{EllipticE}(e_{N-1})$ denotes the complete elliptic integral with the form [42]

$$\mathrm{EllipticE}(e_{N-1}) = \int_0^1 \frac{\sqrt{-e_{N-1}^2t^2+1}}{\sqrt{-t^2+1}}\mathrm{d}t \tag{18}$$

When the thrust acceleration is applied along the tangent direction, the variation of the eccentricity is derived, as follows

$$\begin{aligned} e_N &= e_{N-1} + \Delta e_N \\ \Delta e_N &= \frac{2a_t a_{N-1}^2(1-e_{N-1}^2)^2}{\mu} \\ &\quad \int_0^{2\pi} \frac{e_{N-1}+\cos f}{(1+e_{N-1}\cos f)^2\sqrt{1+e_{N-1}^2+2e_{N-1}\cos f}}\mathrm{d}f \end{aligned} \tag{19}$$

The closed-form solution for Equation (19) can be expressed as

$$\begin{aligned} &\int \frac{e+\cos f}{(1+e\cos f)^2\sqrt{1+e^2+2e\cos f}}\mathrm{d}f \\ &= \frac{1}{-1+e^2}\left(-\frac{1}{e}\mathrm{i}\sqrt{(1+e)^2}\mathrm{EllipticE}\left(\mathrm{i}\sinh^{-1}(\tan(\frac{f}{2}))|\frac{(e-1)^2}{(e+1)^2}\right)\right. \\ &+ 4\mathrm{i}\frac{1}{\sqrt{(1+e)^2}}\mathrm{EllipticPi}\left(\frac{1-e}{1+e};\mathrm{i}\sinh^{-1}(\tan(\frac{f}{2}))|\frac{(e-1)^2}{(e+1)^2}\right) \\ &\left.+\frac{(e-1)\tan\left(\frac{f}{2}\right)\left(e^2+2e\cos(f)+1\right)}{e(e\cos(f)+1)}\right) \end{aligned} \tag{20}$$

where $\mathrm{EllipticE}(\phi|m)$ and $\mathrm{EllipticPi}(n;\phi|m)$ are the complete elliptic integrals of the second kind and the third kind, respectively, which can be obtained in [42].

By combining Equation (16) with Equation (19), we can design an iterative algorithm, as shown in Algorithm 1, to obtain the approximations of the secular variation maxima of the semi-major axis and the consequent variation of the eccentricity.

**Algorithm 1:** Iterative algorithm.

**Input:**
Initial orbital elements $a_0, e_0, i_0, \Omega_0$, and $\omega_0$
**For each loop iteration of each subsection:**
1. Calculate the variation maxima $\Delta \boldsymbol{x}_N$ over one orbital revolution
2. Add the variations of the orbital elements $\boldsymbol{x}_N = \Delta \boldsymbol{x}_N + \boldsymbol{x}_{N-1}$

**Stopping conditions:**
The time of flight reaches the given value.
**Output:**
Approximations for the variation of the orbital elements $\boldsymbol{x}_N$

### 3.2. Secular Variation Maximum of Eccentricity

Two spherical angles $\alpha$ and $\beta$ are introduced to represent the propulsive acceleration vector, as shown in Equation (21). The out-of-plane (yaw) steering angle $\beta$ is measured from the orbit plane to the thrust vector. The in-plane thrust-steering angle $\alpha$ is measured from the velocity vector to the projection of the thrust vector onto the orbit plane [43]. Therefore, the three components of the propulsive acceleration vector are expressed by

$$\begin{aligned} a_t &= a_{\max} \cos\beta \cos\alpha \\ a_n &= a_{\max} \cos\beta \sin\alpha \\ a_h &= a_{\max} \sin\beta \end{aligned} \tag{21}$$

Some researchers have derived the optimal thrust angle that maximizes the rate of the change of the orbital elements [43–45]. By applying the optimal control theory, one can deduce the optimal thrust angles that maximize the change rate of each orbital element. Specifically, they satisfy $\partial\dot{x}/\partial\alpha^* = 0$ and $\partial\dot{x}/\partial\beta^* = 0$. Then, the optimal control profile to maximize the eccentricity is obtained as $\beta^* = 0$. Meanwhile, the optimal thrust angle $\alpha^*$ satisfies

$$\begin{aligned} \sin\alpha^* &= \frac{B_e}{\sqrt{A_e^2 + B_e^2}} \\ \cos\alpha^* &= \frac{A_e}{\sqrt{A_e^2 + B_e^2}} \end{aligned} \tag{22}$$

where the parameters $A_e$ and $B_e$ hold the forms

$$\begin{aligned} A_e &= 2(e + \cos f) \\ B_e &= -\frac{r}{a} \sin f \end{aligned} \tag{23}$$

Furthermore, combining the optimal control profile in Equation (22) with Equations (11) and (21), the variation maximum of the eccentricity over the $N$-th orbital revolution is obtained as

$$\Delta e_N = \frac{a_{\max} a_{N-1}^2 (1 - e_{N-1}^2)^2}{\mu} \int_0^{2\pi} \frac{\sqrt{A_{e,N-1}^2 + B_{e,N-1}^2}}{\rho_{N-1}^2 \sqrt{1 + e_{N-1}^2 + 2e_{N-1}\cos f}} \mathrm{d}f \tag{24}$$

In Equation (24), $A_{e,N-1}$ and $B_{e,N-1}$ represent the values of the parameters $A_e$ and $B_e$ corresponding to the revolution number $N-1$, respectively. Meanwhile, the parameter $\rho_{N-1}$ is defined as $1 + e_{N-1}\cos f$. Then, substituting the optimal control profile in Equation (22) into Equation (10) yields the variation of the semi-major axis over one revolution

$$\Delta a_N = \frac{2 a_{\max} a_{N-1}^3 (1 - e_{N-1}^2)}{\mu} \int_0^{2\pi} \frac{A_{e,N-1} \sqrt{1 + e_{N-1}^2 + 2e_{N-1}\cos f}}{\sqrt{A_{e,N-1}^2 + B_{e,N-1}^2}\, \rho_{N-1}^2} \mathrm{d}f \tag{25}$$

The optimal control Equation (22) that maximizes the variation of the eccentricity leads to the variation equation of the argument of periapsis in the following form

$$\begin{aligned} \frac{\mathrm{d}\omega}{\mathrm{d}f} = & \frac{a_{\max} a^2 (1 - e^2)^2}{\mu e (1 + e\cos f)^2 \sqrt{1 + e^2 + 2e\cos f}} \\ & \left( \frac{2\sin f A_e}{\sqrt{A_e^2 + B_e^2}} + (2e + \frac{1 - e^2}{1 + e\cos f}) \frac{B_e}{\sqrt{A_e^2 + B_e^2}} \right) \end{aligned} \tag{26}$$

As the above equation with respect to the true anomaly is an odd function, thus the variation of the argument of periapsis in each orbital revolution is equal to zero. Then, it satisfied that $\Delta\omega = 0$, and $\omega_N = \omega_0$.

The two integral parts in Equations (24) and (25), respectively, have no analytical primitive functions; however, they can be expanded in a power series in the eccentricity. Thus, the polynomial approximations $P_e(e) = \sum_{k=0}^{4} p_{e,k} e^k$ and $P_a(e) = \sum_{k=0}^{4} p_{a,k} e^k$ are employed to represent the two integrals. The analytical expressions of the variations of the eccentricity and the semi-major axis are expressed as:

$$\begin{aligned} \Delta e_N &= \frac{a_{\max} a_{N-1}^2}{\mu} P_e(e_N) \\ \Delta a_N &= \frac{2 a_{\max} a_{N-1}^3}{\mu} P_a(e_N) \end{aligned} \tag{27}$$

Using the Equation (27), one can obtain the secular approximation of the upper bound for the eccentricity $\Delta e_N$ by applying the iterative algorithm in Algorithm 1. The consequent variation of the semi-major axis can be obtained as well.

### *3.3. Secular Variation Maximum of Inclination*

It can be inferred from Equation (12) that the variation of orbital inclination only depends on the normal acceleration $a_h$. Therefore, the other two components of the propulsive acceleration vector are set to zero. Accordingly, the semi-major axis and the eccentricity are invariant, i.e., $a = a_0$ and $e = e_0$, and the differential equation of the inclination becomes

$$\frac{\mathrm{d}i}{\mathrm{d}f} = \frac{a_h p_0^2}{\mu} \frac{\cos\theta}{(1 + e_0 \cos f)^3} \tag{28}$$

The optimal control profile $a_h$ to maximize the inclination variation has two parts: the direction and the magnitude. The magnitude is always equal to $a_{\max}$. Since the value of $\cos\theta$ changes periodically, the sign of $a_h$ within one revolution will be switched according to the instantaneous value of $\cos\theta$. Therefore, the optimal control profile to maximize the variation of the inclination is founded by

$$\begin{aligned} &|a_h| = a_{\max} \\ &\operatorname{sgn}(a_h) = \begin{cases} 1 & \theta \in [2k\pi - \frac{\pi}{2}, 2k\pi + \frac{\pi}{2}] \\ -1 & \theta \in [2k\pi + \frac{\pi}{2}, 2k\pi + \frac{3\pi}{2}] \end{cases} \end{aligned} \tag{29}$$

where the parameter $k \in Z$ represents an arbitrary integer. The variation maximum of the inclination over one revolution can be integrated directly.

$$\begin{aligned} \Delta i = &\frac{a_{\max} \cos\omega p_0^2}{\mu} \int_0^{2\pi} \frac{\operatorname{sgn}(a_h) \cos f}{(1 + e_0 \cos f)^3} \mathrm{d}f \\ &- \frac{a_{\max} \sin\omega p_0^2}{\mu} \int_0^{2\pi} \frac{\operatorname{sgn}(a_h) \sin f}{(1 + e_0 \cos f)^3} \mathrm{d}f \end{aligned} \tag{30}$$

These two integrals in Equation (30) have general analytical primitive functions, which are expressed in terms of the eccentric anomaly $E$ [46]

$$\begin{aligned} H &= \int_{f_0}^{f} \frac{\cos f}{(1 + e\cos f)^3} \mathrm{d}f \\ &= -\left(1 - e^2\right)^{-\frac{5}{2}} \times \left[\frac{3eE}{2} - \left(1 + e^2\right)\sin E + \frac{e}{4}\sin 2E - (\frac{3eE_0}{2} - \left(1 + e^2\right)\sin E_0 + \frac{e}{4}\sin 2E_0)\right] \\ G &= \int_{f_0}^{f} \frac{\sin f}{(1 + e\cos f)^3} \mathrm{d}f \\ &= (1 - e^2)^{-2}\left(-\cos E + \frac{e}{4}\cos 2E + \cos E_0 - \frac{e}{4}\cos 2E_0\right) \end{aligned} \tag{31}$$

Here, we use the $H_i$ and $G_i$ to denote the primitive functions of the two integrals in Equation (30). The variation maximum of the inclination over one revolution can be written as

$$\Delta i = \frac{a_{\max} \cos \omega p_0^2}{\mu} H_i - \frac{a_{\max} \sin \omega p_0^2}{\mu} G_i \tag{32}$$

Meanwhile, the variational equations of the right ascension of the ascending node and the argument of periapsis under the optimal control profile (29) are expressed as

$$\begin{aligned} \frac{\mathrm{d}\Omega}{\mathrm{d}f} &= \frac{a_h p_0^2}{\mu \sin i} \frac{\sin(\omega + f)}{(1 + e \cos f)^3} \\ \frac{\mathrm{d}\omega}{\mathrm{d}f} &= -\cos i \frac{\mathrm{d}\Omega}{\mathrm{d}f} \end{aligned} \tag{33}$$

As the variation maximum of the inclination is obtained analytically, we will propose two strategies with different computational efficiency and accuracy to solve for the secular variation maximum of the inclination.

3.3.1. Strategy 1

The variation of the argument of the periapsis is small when investigating the variation maximum of the inclination. Therefore, it can be ignored to obtain an explicit analytical solution. When the argument of periapsis remains unchanged, the variation maximum of the inclination and the variation of $\Omega$ and $\omega$ are represented as

$$\begin{aligned} \Delta i &= \frac{a_{\max} \cos \omega_0 p_0^2}{\mu} H_i - \frac{a_{\max} \sin \omega_0 p_0^2}{\mu} G_i = \text{const} \\ \Delta \Omega &= \frac{a_h p_0^2 \sin \omega_0}{\mu \sin i} H_i + \frac{a_h p_0^2 \cos \omega_0}{\mu \sin i} G_i = \text{const} \\ \Delta \omega &= 0 \end{aligned} \tag{34}$$

Similarly, the differential equations for the variation maxima of the inclination and the right ascension of the ascending node, with respect to the number of orbital revolutions, are given as

$$\begin{aligned} \frac{\mathrm{d}i}{\mathrm{d}N} &= C_i \\ \frac{\mathrm{d}\Omega}{\mathrm{d}N} &= \frac{C_\Omega}{\sin(i)} \end{aligned} \tag{35}$$

where $C_i = \Delta i$ and $C_\Omega$ are both constant. Meanwhile, $C_\Omega$ holds the form

$$C_\Omega = \frac{a_h p_0^2 \sin \omega_0 H_\Omega}{\mu} + \frac{a_h p_0^2 \cos \omega_0 G_\Omega}{\mu} \tag{36}$$

We can solve the differential equations (35) for the variation maximum of inclination and the consequent variations of the right ascension of the ascending node. They are of the forms

$$\begin{aligned} i_N &= i_0 + C_i N \\ \Omega_N &= \Omega_0 + \frac{C_\Omega}{C_i} [\ln(\tan \frac{i_0 + C_i N}{2}) - \ln(\tan \frac{i_0}{2})] \end{aligned} \tag{37}$$

This shows that the maximum of the inclination increases linearly under the normal propulsive acceleration.

3.3.2. Strategy 2

For a higher accuracy, we take the small variation of the argument of periapsis into account. The variations of $i, \Omega$ and $\omega$ over one revolution are expressed as

$$\begin{aligned}\Delta i_N &= \frac{a_{\max}\cos\omega_{N-1}p_0^2}{\mu}H_i - \frac{a_{\max}\sin\omega_{N-1}p_0^2}{\mu}G_i \\ \Delta\Omega_N &= \frac{a_h p_0^2\sin\omega_{N-1}}{\mu\sin i_{N-1}}H_i + \frac{a_h p_0^2\cos\omega_{N-1}}{\mu\sin i_{N-1}}G_i \\ \Delta\omega_N &= -\cos i_{N-1}\Delta\Omega_N\end{aligned} \tag{38}$$

The variations of $i, \Omega$, and $\omega$ over one revolution are obtained analytically by Equation (38). The secular variation maximum of the inclination and the variations of the right ascension of the ascending node and the argument of periapsis can be obtained through the iterative algorithm given in Algorithm 1.

*3.4. Secular Variation Maximum of Right Ascension of the Ascending Node*

Similar to the approximation of the inclination, the variation of the right ascension of the ascending node depends only on the normal acceleration $a_h$. Meanwhile, $a = a_0$ and $e = e_0$ are still satisfied. The variational Equation (13) is rewritten as

$$\frac{\mathrm{d}\Omega}{\mathrm{d}f} = \frac{a_h p_0^2}{\mu\sin i}\frac{\sin(\omega_0+f)}{(1+e\cos f)^3} \tag{39}$$

To maximize the variation of the right ascension of the ascending node over one orbital revolution, the magnitude of the acceleration in the norm direction should achieve its maximum $a_{\max}$. When the inclination angle is equal to 0 or $\pi$, the variational equations will be singular. Therefore, the inclination range, $(0, \pi)$, is considered to avoid the singularities. Then, the sign of $a_h$ depends on the value of the sine function $\sin(\omega_0 + f)$. Consequently, the optimal control profile to maximize the variation of $\Omega$ is derived as

$$\begin{aligned}&|a_h| = a_{\max} \\ &\mathrm{sgn}(a_h) = \begin{cases} 1 & \theta \in [2k\pi, 2k\pi+\pi] \\ -1 & \theta \in [2k\pi+\pi, 2(k+1)\pi] \end{cases}\end{aligned} \tag{40}$$

Substituting the optimal control profile (40) into the differential Equation (39), results in the variation maximum of the right ascension of the ascending node $\Delta\Omega$ over one revolution. The method to maximize the right ascension of the ascending node is same as the one to maximize the inclination. The only difference is that the optimal control profiles (40) and (29) are applied, respectively. Therefore, the secular maximum of the right ascension of the ascending node can be obtained by Equations (37) and (38) from the two strategies proposed in Section 3.3. Meanwhile, the consequent variations of the inclination and the argument of periapsis are obtained as well.

The approximation of the right ascension of the ascending node in the previous part of this subsection is obtained, assuming no other orbital perturbation acceleration is considered except the low-thrust acceleration. In the low-Earth orbit, the variations of $\Omega$ and $\omega$ caused by the second order zonal harmonic of the Earth's gravitational potential, $J_2$, are not small enough. In the next part of this subsection, the variation maximum of the right ascension of the ascending node is conducted by considering the $J_2$ perturbation and the low-thrust acceleration.

The variational equations for the orbit elements, $\boldsymbol{x} = [a, e, i, \Omega, \omega]$, considering the low thrust acceleration and the $J_2$ perturbation, can be expressed as $\mathrm{d}\boldsymbol{x}/\mathrm{d}t = \mathrm{d}\boldsymbol{x}_{LT}/\mathrm{d}t + \mathrm{d}\boldsymbol{x}_{J_2}/\mathrm{d}t$, where $\mathrm{d}\boldsymbol{x}_{LT}/\mathrm{d}t$ and $\mathrm{d}\boldsymbol{x}_{J_2}/\mathrm{d}t$ represent the components of the variational equations under the low-thrust acceleration and the $J_2$ perturbation, respectively, and $\mathrm{d}\boldsymbol{x}_{LT}/\mathrm{d}t$ holds

the form in Equations (1)–(6). Neglecting the short-term effect of the $J_2$ perturbation, one can obtain the variational equations $\mathrm{d}\boldsymbol{x}_{J_2}/\mathrm{d}t$ [47].

$$\begin{aligned}
\frac{\mathrm{d}a_{J_2}}{\mathrm{d}t} &= \frac{\mathrm{d}e_{J_2}}{\mathrm{d}t} = \frac{\mathrm{d}i_{J_2}}{\mathrm{d}t} = 0 \\
\frac{\mathrm{d}\Omega_{J_2}}{\mathrm{d}t} &= -\frac{3}{2}J_2\sqrt{\mu}\left(\frac{R_E}{1-e^2}\right)^2 a^{-\frac{7}{2}}\cos i \\
\frac{\mathrm{d}\omega_{J_2}}{\mathrm{d}t} &= \frac{3}{2}J_2\sqrt{\mu}\left(\frac{R_E}{1-e^2}\right)^2 a^{-\frac{7}{2}}\left(2-\frac{5}{2}\sin^2 i\right)
\end{aligned} \tag{41}$$

where $J_2 = 1.08262668 \times 10^{-3}$ is the coefficient of the flattening perturbation and $R_E = 6{,}378{,}137$ m. The average changes of the orbital elements $a$, $e$, and $i$ caused by the $J_2$ perturbation per orbit are null.

The variation maximum of $\Omega$ and the consequent variations of $i$ and $\omega$ over one orbital revolution, considering the effect of the low-thrust acceleration and the $J_2$ perturbation, hold the form

$$\begin{aligned}
\Delta\Omega_N &= \Delta\Omega_{LT,N} + \Delta\Omega_{J_2,N} \\
\Delta i_N &= \Delta i_{LT,N} + \Delta i_{J_2,N} \\
\Delta\omega_N &= \Delta\omega_{LT,N} + \Delta\omega_{J_2,N}
\end{aligned} \tag{42}$$

where $\Delta\Omega_{LT,N}$, $\Delta i_{LT,N}$, and $\Delta\omega_{LT,N}$ donate the variations over one revolution caused by the given optimal control low thrust expressed in Equation (40). $\Delta\Omega_{LT,N}$, $\Delta i_{LT,N}$, and $\Delta\omega_{LT,N}$ donate the variations caused by the $J_2$ perturbation over one revolution, and they can be derived as

$$\begin{aligned}
\Delta\Omega_{J_2,N} &= -3\pi J_2\left(\frac{R_E}{a_0(1-e_0^2)}\right)^2\cos i_{N-1} \\
\Delta i_{J_2,N} &= 0 \\
\Delta\omega_{J_2,N} &= 3\pi J_2\left(\frac{R_E}{a_0(1-e_0^2)}\right)^2\left(2-\frac{5}{2}\sin^2 i_{N-1}\right)
\end{aligned} \tag{43}$$

We can obtain the secular variation maximum of the right ascension of the ascending node, as well as the consequent variation of the inclination and the argument of periapsis, by combining the Equation (42) and the iterative algorithm given in Algorithm 1.

### *3.5. Secular Variation Maximum of Argument of Periapsis*

The variation of the argument of periapsis depends on all the three components of the propulsive acceleration vector. Thus, Equations (21) are used to represent the acceleration vector. By substituting Equation (21) into Equation (14), we can derive the parameterized differential equation of the argument of periapsis.

$$\frac{\mathrm{d}\omega}{\mathrm{d}f} = \frac{a_{\max}p^2}{h(1+e\cos f)^2}\left(A\cos\beta\cos\alpha + B\cos\beta\sin\alpha + C\cos\beta\right)) \tag{44}$$

where

$$\begin{aligned}
A &= \frac{1}{ev}2\sin f \\
B &= \frac{1}{ev}\left(2e+\frac{r}{a}\cos f\right) \\
C &= -\frac{r\sin\theta\cos i}{h\sin i}
\end{aligned} \tag{45}$$

As the term $\frac{r^2}{h}$ in Equation (44) is always positive, one can deduce the optimal thrust angles by applying the optimal control theory.

$$\begin{aligned}\cos\alpha^* &= \frac{A}{\sqrt{A^2+B^2}}\\ \sin\alpha^* &= \frac{B}{\sqrt{A^2+B^2}}\\ \cos\beta^* &= \frac{\sqrt{A^2+B^2}}{\sqrt{A^2+B^2+C^2}}\\ \sin\beta^* &= \frac{C}{\sqrt{A^2+B^2+C^2}}\end{aligned} \tag{46}$$

Substituting the optimal control profile (46) into Equation (44), we can obtain the variation maximum of the argument of periapsis over one revolution.

$$\Delta\omega_{LT,N} = \int_0^{2\pi} \frac{a_{\max} p_{N-1}^2}{h_{N-1}} \frac{\sqrt{A_{N-1}^2 + B_{N-1}^2 + C_{N-1}^2}}{(1+e_{N-1}\cos f)^2} \mathrm{d}f \tag{47}$$

The consequent variations of the other orbital elements over one revolution can also be obtained by applying the control profile (46). Then, by using the designed iterative algorithm in Algorithm 1, we can obtain the secular variation maximum of the argument of periapsis and the consequent variations of the other elements.

Two primary additional analysis can also be performed. First, a correction for the variation of the argument of periapsis over one revolution is conducted. The variation with the time of the argument of latitude is [11]

$$\frac{\mathrm{d}\omega}{\mathrm{d}t} + \frac{\mathrm{d}f^{\mathrm{real}}}{\mathrm{d}t} = \frac{h}{r^2} - \frac{r\sin(\omega+f)\cos i}{h\sin i} \approx \frac{h}{r^2} \tag{48}$$

where the $f^{\mathrm{real}}$ denotes the exact value of the true anomaly. The approximation in Equation (48) is based on the assumption that the normal acceleration is small enough to produce a negligible effect. By dividing Equation (48) by the assumption in Equation (9), the following expression can be derived.

$$\frac{\mathrm{d}f^{\mathrm{real}}}{\mathrm{d}f} \approx 1 - \frac{\mathrm{d}\omega}{\mathrm{d}f} \tag{49}$$

The following expression can be obtained by integrating the Equation (49).

$$\Delta f^{\mathrm{real}} = 2\pi - \Delta\omega_{LT,N} \tag{50}$$

The variation maximum of the argument of periapsis over one revolution with a correction, denoted by $\Delta\omega_N^{\mathrm{cor}}$, can be obtained by the linear interpolation as

$$\Delta\omega_{LT,N}^{\mathrm{cor}} = \frac{2\pi}{2\pi - \Delta\omega_N}\Delta\omega_{LT,N} \tag{51}$$

Second, parameter $K = \frac{\max(A^2+B^2)}{\max(C^2)}$ is used to evaluate the magnitude ratio of $A^2+B^2$ to $C^2$. The parameter $K$ can be expanded in the power series in the eccentricity. The approximation of $K$ can be expressed as $K \approx 4/(e^2\cot^2 i)$. Its values for different eccentricity and inclination are shown in Figure 3. It can be inferred that the smaller the eccentricity and the closer the inclination to $\pi/2$, the bigger the value of $K$. To some extent, the parameter $K$ indicates the effect of the acceleration component $a_h$ on the variation maximum of the argument of periapsis. Combining the Equation (21) and the optimal thrust angle in Equation (46), the bigger the value of $K$ is, the closer the applied acceleration $a_h$ is to zero.

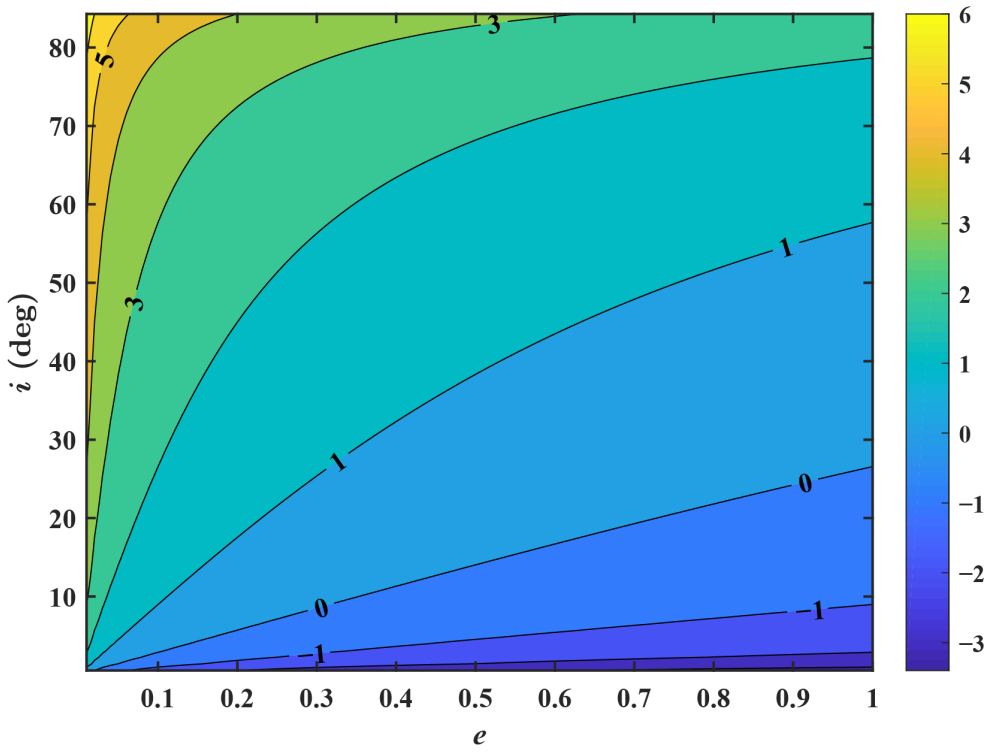


**Figure 3.** Value of parameter $\log_{10} K$ for different inclination and eccentricity.

When the value of $K$ is large, $A^2 + B^2 + C^2 \approx A^2 + B^2$, and the acceleration component $a_h$ is small and ignored. Then, the optimal control profile is transferred as

$$\begin{aligned} a_t^* &= a_{\max} \frac{A}{\sqrt{A^2 + B^2}} \\ a_n^* &= a_{\max} \frac{B}{\sqrt{A^2 + B^2}} \\ a_h^* &= 0 \end{aligned} \tag{52}$$

Substituting the simplified optimal control profile into Equations (10)–(14), we can find that the variational equations of the semi-major axis and the eccentricity are odd functions. Thus, their variations over one revolution are zero. Meanwhile, the variation of the inclination and the right ascension of the ascending node are small and ignored. Therefore, $a = a_0, e = e_0, i = i_0, \Omega = \Omega_0$, and the variation of the argument of periapsis over one revolution is simplified as

$$\Delta\omega_{LT,N} = \int_0^{2\pi} \frac{a_{\max} p_0^2}{h_0} \frac{\sqrt{A_0^2 + B_0^2}}{(1 + e_0 \cos f)^2} \mathrm{d}f = \text{const} \tag{53}$$

It means that the variation maximum of the argument of periapsis caused by the low-thrust acceleration is constant over each revolution when the parameter $K$ is large.

From the former parts of this subsection, we can obtained the variation maximum of the argument of periapsis caused by the low-thrust acceleration. Meanwhile, the variation caused by the $J_2$ perturbation has been derived in Equation (43). By using the formulas in Equation (42) and the iterative algorithm given in Algorithm 1, we can now obtain the secular variation maximum of the argument of periapsis, considering both the low-thrust acceleration and the $J_2$ perturbation.

## 4. Numerical Simulations

In the first part of this section, the optimization model of the indirect method is established. To validate the optimality of the indirect method, we conducted several simulations to compare the solutions to those obtained by GPOPS version 1.0 [48], which is a MATLAB software for solving multiple-phase optimal control problems using the Gauss pseudospectral method. Meanwhile, simulations for the variation maxima of the orbital elements over a fixed flight time are conducted to demonstrate the efficiency and accuracy of the proposed method compared with the indirect method. Then, a preliminary application of the proposed method is conducted to estimate the velocity increments of orbital transfers. All the simulations are coded in C++ and performed on a personal desktop with an Intel Core i7-7700 CPU of 3.6 GHz and 16.00 GB of RAM.

### *4.1. Simulations for Variation Maximum of Each Orbital Element*

In this study, the approximation solutions obtained by the proposed method are compared with those by an indirect method. The optimization model is established first by considering the mass consumption. The nonlinear optimal control model that maximizes the variation maximum of the semi-major axis over a fixed flight time is taken as an example and given as follows.

Minimize:

$$J = -a(tf) \tag{54}$$

Subject to

$$\begin{aligned} \dot{\boldsymbol{X}}(t) &= \boldsymbol{f}(\boldsymbol{X}, \boldsymbol{u}, m, t) \\ \dot{m}(t) &= -\frac{T_{\max} u}{I_{\mathrm{sp}} g_0} \\ \boldsymbol{X}(t_0) &= \boldsymbol{X}_0, m(t_0) = m_0 \end{aligned} \tag{55}$$

where $\boldsymbol{u}$ denotes the control vector, $\boldsymbol{u} = \frac{T_{\max} u}{m} \boldsymbol{\alpha}$. $\boldsymbol{\alpha}$ is an unit vector and denotes the direction of the control vector. The engine thrust ratio is $u \in [0, 1]$. The state $\boldsymbol{X}$ represents $\boldsymbol{X} = [a, e, i, \Omega, \omega, f]^{\mathrm{T}}$. The right-hand side of the first equation in Equation (55) represents Gauss's variational equations in Equations (1)–(6), and it holds the form as $\boldsymbol{f}(\boldsymbol{X}, \boldsymbol{u}, m, t) = \boldsymbol{M}\boldsymbol{u}$. The final conditions are expressed as

$$\begin{aligned} &\boldsymbol{X}(t_f) = [a(t_f), e(t_f), i(t_f), \Omega(t_f), \omega(t_f), f(t_f)]^{\mathrm{T}} = \text{free} \\ &m(t_f) = \text{free} \\ &\text{ToF} = t_f - t_0 \end{aligned} \tag{56}$$

First, by introducing the costate vector $\boldsymbol{\lambda} = [\boldsymbol{\lambda}_{\boldsymbol{X}}, \lambda_m]$, which is known as the functional Lagrange multiplier, the Hamiltonian is built as [49]

$$H = \boldsymbol{\lambda}_{\boldsymbol{X}}^{\mathrm{T}} \boldsymbol{M}\boldsymbol{u} - \lambda_m \frac{T_{\max}}{I_{\mathrm{sp}} g_0} u \tag{57}$$

The costate differential equations that are termed as Euler-Lagrange equations are given as $\dot{\boldsymbol{\lambda}}_{\boldsymbol{X}} = -\partial H / \partial \boldsymbol{X}$ and $\dot{\lambda}_m = -\partial H / \partial m$. By applying the optimal control theory [50], we can obtain the final costate $\boldsymbol{\lambda}(tf) = \frac{\partial(-a(t_f))}{\partial \boldsymbol{X}(t_f)} = [-1, 0, 0, 0, 0, 0]^{\mathrm{T}}$, and the final mass costate $\lambda_m(tf) = \frac{\partial(-a(t_f))}{\partial m(tf)} = 0$.

The optimal thrust direction and magnitude, which minimize the Hamiltonian, are determined by [49]

$$\begin{aligned} u &= 1 \\ \boldsymbol{\alpha} &= -\frac{\boldsymbol{M}^{\mathrm{T}} \boldsymbol{\lambda}_{\boldsymbol{X}}}{||\boldsymbol{M}^{\mathrm{T}} \boldsymbol{\lambda}_{\boldsymbol{X}}||} \end{aligned} \tag{58}$$

Given the initial costates $\boldsymbol{\lambda}(t_0)$ and the initial state in Equation (55), we can obtain the final states and costates by integrating the differential equations of the states and costates. Meanwhile, the final states are free and the final costates should satisfy their final values. Therefore, the optimal control problem yields a two-point boundary value problem consisting of a set of equations of the form:

$$\boldsymbol{\Phi} = [\boldsymbol{\lambda}_{\boldsymbol{X}}(t_f), \lambda_m(t_f)]^{\mathrm{T}} - [-1, 0, 0, 0, 0, 0, 0]^{\mathrm{T}} = \mathbf{0} \tag{59}$$

where Equation (59) is called the shooting function. MinPack-1 [51], a package of FORTRAN subprograms for the numerical solution of the systems of nonlinear equations and nonlinear least-squares problems is used here to solve the shooting functions in the indirect method. Then, we can obtain the variation maximum over a finite flight time of the semi-major axis. Meanwhile, the solution of the indirect method in solving the variation maxima of the other elements can be also obtained in this way, but is omitted here for the sake of conciseness.

Four numerical simulation cases including three geocentric orbital transfers and one heliocentric orbital transfer are given to substantiate the proposed method. In each case, the simulation of approximating the secular variation maximum of each orbital element is carried out individually. The spacecraft parameters are selected as $P_{\max} = 2.86\,\mathrm{kW}$, $\eta = 0.6$, and $I_{\mathrm{sp}} = 3500$ s from a NEXT engine [40], and the initial mass is $m_0 = 1000\,\mathrm{kg}$. Thus, the constant acceleration magnitude is $a_{\max} = 10^{-4}\,\mathrm{m/s^2}$, corresponding to the mass-flow rate $2.91 \times 10^{-6}$ kg/s. The fixed flight times are set to 50 days and 400 days for cases 1–3 and case 4, respectively. The mean equatorial radius of the Earth, $R_E$, is used to normalize the values of the semi-major axis in cases 1–3. The astronomical unit, AU, is used in case 4. The simulation parameters with a wide range of initial orbital elements are listed in Table 1. The eccentricity is near singularity in case 1 and the thrust-to-gravity ratio is large in case 4. The variation maxima of the argument of periapsis are very huge over a short flight time, being much lower than 50 days in both of these two cases. Therefore, the simulations for argument of periapsis in case 1 and case 4 are omitted.

**Table 1.** Parameters for initial orbital elements.

| Case | $a_0$ | $e_0$ | $i_0$, deg | $\Omega_0$, deg | $\omega_0$, deg | $f_0$, deg |
|---|---|---|---|---|---|---|
| 1 | 1.1759, $R_E$ | 0.001 | 10 | 30 | 10 | 0 |
| 2 | 3.9196, $R_E$ | 0.5 | 55 | 150 | 130 | 0 |
| 3 | 5.8011, $R_E$ | 0.3 | 100 | 270 | 250 | 0 |
| 4 | 1.0, AU | 0.0167 | 5 | 30 | 50 | 0 |

As shown in Table 2, the solutions produced by the indirect method for case 3 are compared with those of GPOPS. The percentage errors are on the order of one-thousandth. It indicates that when solving the secular variations of orbital elements, the performance of the indirect method is comparable to that of GPOPS in terms of the optimality. Although GPOPS is a powerful MATLAB software for solving multiple-phase optimal control problems, good initial guesses of the state and control are also needed to guarantee the convergence and to obtain a good local optimal solution. In this paper, the solutions of the indirect method are used as references to compare with those of the proposed method.

**Table 2.** Comparison of the solutions solved by GPOPS and the indirect method for Case 3.

| Case 3 | $a_f$, $R_E$ | $e_f$ | $i_f$, deg | $\Omega_f$, deg | $\omega_f$, deg |
|---|---|---|---|---|---|
| Indirect method | 7.6628 | 0.4875 | 104.9775 | 275.8517 | 291.4525 |
| GPOPS | 7.6775 | 0.4837 | 105.0753 | 275.8700 | 290.1070 |
| Percentage error | $1.9 \times 10^{-3}$ | $7.8 \times 10^{-3}$ | $9.3 \times 10^{-4}$ | $6.6 \times 10^{-5}$ | $4.6 \times 10^{-3}$ |

The computational times spent by the proposed method and the indirect method are listed in Table 3. The numbers after S1 and S2 are the computational times of the strategy 1 and 2 proposed in Section 3.3. The subscripted symbols represent the computational times. For example, $t_a$ represents the computational time in solving the variation maximum of the semi-major axis. It shows that the propose method spends tens of microseconds to obtain a variation maximum of one orbital element and the indirect method spends several seconds in general. Due to the limited number of orbital revolutions in case 4, both of the two methods require less computational time than they do in the other cases. Compared with the numerical indirect method, the proposed method greatly saves the computational time. In general, the computational time for approximating the secular variation maximum of each orbital element could be reduced by over five orders of magnitude. The computational times for solving the variational maxima by the proposed strategy 1 are reduced by over seven orders of magnitude.

**Table 3.** Computational times.

| | **Proposed Method** | | | | | **Indirect Method** | | | | |
|---|---|---|---|---|---|---|---|---|---|---|
| **Case** | $t_a$, $\times 10^{-5}$ **s** | $t_e$, $\times 10^{-5}$ **s** | $t_i$, $\times 10^{-5}$ **s** | $t_\Omega$, $\times 10^{-5}$ **s** | $t_\omega$, $\times 10^{-5}$ **s** | $t_a$, **s** | $t_e$, **s** | $t_i$, **s** | $t_\Omega$, **s** | $t_\omega$, **s** |
| 1 | 6.2 | 7.3 | S1: 0.08<br>S2: 20 | S1: 0.04<br>S2: 19 | / | 25.64 | 4.58 | 150.73 | 6.91 | / |
| 2 | 1.1 | 1.2 | S1: 0.05<br>S2: 3.3 | S1: 0.06<br>S2: 3.2 | 10 | 10.19 | 71.48 | 1.51 | 5.84 | 16.07 |
| 3 | 1.0 | 0.7 | S1: 0.09<br>S2: 1.9 | S1: 0.08<br>S2: 1.9 | 20 | 1.44 | 15.65 | 1.15 | 9.02 | 27.67 |
| 4 | 0.093 | 0.016 | 0.011 | 0.083 | / | 0.036 | 0.032 | 0.082 | 0.367 | / |

The variation maxima of orbital elements over a fixed flight time are listed in Table 4. The results obtained by the proposed method are slightly less than those by the indirect method. The indirect method provides better solutions of the variation maxima with longer computational times. Compared with the indirect method, the percentage errors of the solutions obtained by the proposed method are on the order of the one-thousandth for cases 1–3. From the approximations for the secular variations of the inclination and the right ascension of the ascending node in cases 1–3, we can find that the accuracies of the two strategies conducted in Section 3.3 are similar, but their computational times are quite different. The approximations for the secular variation maxima of the right ascension of the ascending node considering the $J_2$ perturbation and low thrust by the proposed method are also consistent with the accuracy solutions of the indirect method. In case 2, when the $J_2$ perturbation is taken into account, the variation maximum of the right ascension of the ascending node decreases, while the variation maximum of the periapsis argument grows. These simulation results are consistent with the results of the analysis of Equation (41). In case 2, the signs of the differentials of the right ascension of the ascending node and the argument of periapsis under the $J_2$ perturbation are negative and positive, respectively. On the contrary, in case 3, the $J_2$ perturbation decreases the right ascension of the ascending node and increases the argument of periapsis. Meanwhile, for case 4, which has a higher thrust-to-gravity ratio, the percentage error increases to the order of one percent.

**Table 4.** Variation maxima of the orbital elements over a fixed flight time.

| | $x_f$ | Proposed | Indirect Method | Percentage Error |
|---|---|---|---|---|
| Case 1 | $a_f$, $R_E$ | 1.3287 | 1.3297 | $8.2 \times 10^{-4}$ |
| | $e_f$ | 0.0923 | 0.0928 | $6.3 \times 10^{-3}$ |
| | $i_f$, deg | S1: 12.1615 | 12.1647 | $2.6 \times 10^{-4}$ |
| | | S2: 12.1615 | | $2.6 \times 10^{-4}$ |
| | $\Omega_f$, deg | S1: 42.4473 | 42.6318 | $4.3 \times 10^{-3}$ |
| | | S2: 42.4287 | | $4.7 \times 10^{-3}$ |
| Case 2 | $a_f$, $R_E$ | 4.8558 | 4.8658 | $2.1 \times 10^{-3}$ |
| | $e_f$ | 0.6369 | 0.6376 | $1.1 \times 10^{-3}$ |
| | $i_f$, deg | S1: 59.9658 | 60.1101 | $2.4 \times 10^{-3}$ |
| | | S2: 59.9955 | | $1.9 \times 10^{-3}$ |
| | $\Omega_f$, deg | S1: 156.6328 | 156.9221 | $1.8 \times 10^{-3}$ |
| | | S2: 156.8552 | | $1.6 \times 10^{-3}$ |
| | $\Omega_f(J_2)$, deg | 152.2657 | 152.8683 | $3.9 \times 10^{-3}$ |
| | $\omega_f$, deg | 147.5200 | 147.9650 | $3.0 \times 10^{-3}$ |
| | $\omega_f(J_2)$, deg | 147.5433 | 147.9809 | $2.9 \times 10^{-3}$ |
| Case 3 | $a_f$, $R_E$ | 7.6366 | 7.6628 | $3.4 \times 10^{-3}$ |
| | $e_f$ | 0.4863 | 0.4875 | $2.4 \times 10^{-4}$ |
| | $i_f$, deg | S1: 104.9113 | 104.9775 | $6.3 \times 10^{-4}$ |
| | | S2: 104.9107 | | $6.4 \times 10^{-4}$ |
| | $\Omega_f$, deg | S1: 275.6966 | 275.8517 | $5.6 \times 10^{-4}$ |
| | | S2: 275.6077 | | $8.8 \times 10^{-4}$ |
| | $\Omega_f(J_2)$, deg | 275.8296 | 276.0224 | $6.9 \times 10^{-4}$ |
| | $\omega_f$, deg | 287.4059 | 291.4525 | $13 \times 10^{-3}$ |
| | $\omega_f(J_2)$, deg | 287.3791 | 290.9265 | $12 \times 10^{-3}$ |
| Case 4 | $a_f$, AU | 1.2387 | 1.2684 | $2.6 \times 10^{-2}$ |
| | $e_f$ | 0.1952 | 0.2081 | $6.2 \times 10^{-2}$ |
| | $i_f$, deg | 9.2333 | 9.5141 | $2.9 \times 10^{-3}$ |
| | $\Omega_f$, deg | 78.5656 | 84.9038 | $7.5 \times 10^{-2}$ |

### *4.2. Estimation of the Velocity Increment*

As the variation maxima of the COE of low-thrust spacecraft have been obtained effectively, one application for the proposed method is to estimate the velocity increment of the orbital transfer. Simulations of two minimum-time orbital transfer examples, whose COE are listed in Table 5, are designed to estimate the $\Delta V$. The spacecraft is launched into a middle Earth orbit, and the initial semi-major axis is 27,906 km and the initial inclination is 40 deg. For the example 1, we aim to increase the inclination only. The initial inclination is 40 degrees. The final orbital inclinations range from 42 degrees to 56 degrees. In example 2, we test the orbital transfers from initial orbits with different eccentricities to the targets. The initial eccentricities range from 0.0106 to 0.4106. The increments of the semi-major axis and the inclination between the target orbit and the initial orbit are 3000 km and 5 degrees, respectively.

**Table 5.** Orbit elements of the initial orbit and the target.

| | Example 1 | | Example 2 | |
|---|---|---|---|---|
| **Orbit Elements** | **Initial Orbit** | **Target** | **Initial Orbit** | **Target** |
| Semi-major axis, km | 27,906 | 27,906 | 27,906 | 30,906 |
| Eccentricity | 0.0106 | 0.0106 | 0.0106–0.4106 | free |
| Inclination, deg | 40 | 42–56 | 40 | 45 |

The indirect method is used to solve for the accurate velocity increments for the time optimal orbital transfer problem of the simulation examples. The time optimal problem of the indirect method is modeled for the orbital transfer problem.

Minimize:

$$J = \int_{t_0}^{t_0+\mathrm{ToF}} 1 \mathrm{d}t \tag{60}$$

Subject to

$$\begin{aligned} \dot{\boldsymbol{X}}(t) &= \boldsymbol{f}(\boldsymbol{X}, \boldsymbol{u}, m, t) \\ \dot{m}(t) &= -\frac{T_{\max} u}{I_{\mathrm{sp}} g_0} \\ \boldsymbol{X}(t_0) &= \boldsymbol{X}_0, m(t_0) = m_0 \end{aligned} \tag{61}$$

The final conditions are expressed as

$$\begin{aligned} \text{Example 1}: & \begin{cases} [a(t_f), e(t_f), i(t_f)]^{\mathrm{T}} = [a_0, e_0, i_f]^{\mathrm{T}} \\ [\Omega(t_f), \omega(t_f), f(t_f), m(t_f)]^{\mathrm{T}} = \text{free} \\ \mathrm{ToF} = \text{free} \end{cases} \\ \text{Example 2}: & \begin{cases} [a(t_f), i(t_f)]^{\mathrm{T}} = [a_f, i_f]^{\mathrm{T}} \\ [e(t_f), \Omega(t_f), \omega(t_f), f(t_f), m(t_f)]^{\mathrm{T}} = \text{free} \\ \mathrm{ToF} = \text{free} \end{cases} \end{aligned} \tag{62}$$

By solving the time optimal transfer problem, we can obtain the minimum transfer time $\mathrm{ToF}_I$. Then, the velocity increments are calculated by integrating the immediate propulsive acceleration from $t_0$ to $t_0 + \mathrm{ToF}_I$ as $\Delta V_I = \int_{t_0}^{t_0+\mathrm{ToF}_I} ||\boldsymbol{u}|| \mathrm{d}t$. The percentage error is calculated by $\frac{|\Delta V_P - \Delta V_I|}{\Delta V_I}$. $\Delta V_P = a_{\max} \mathrm{ToF}_P$ represents the velocity increment solved by the proposed method. The $\mathrm{ToF}_P$ is obtained by adding up the transfer time until the desired final orbital elements are reached.

For the inclination increment problem of example 1, the velocity increments estimated by the proposed method and the indirect method are shown in Figure 4. The $\Delta V$ increases with the increase in the inclination. In general, the percentage error grows with the increase in the inclination of the target.

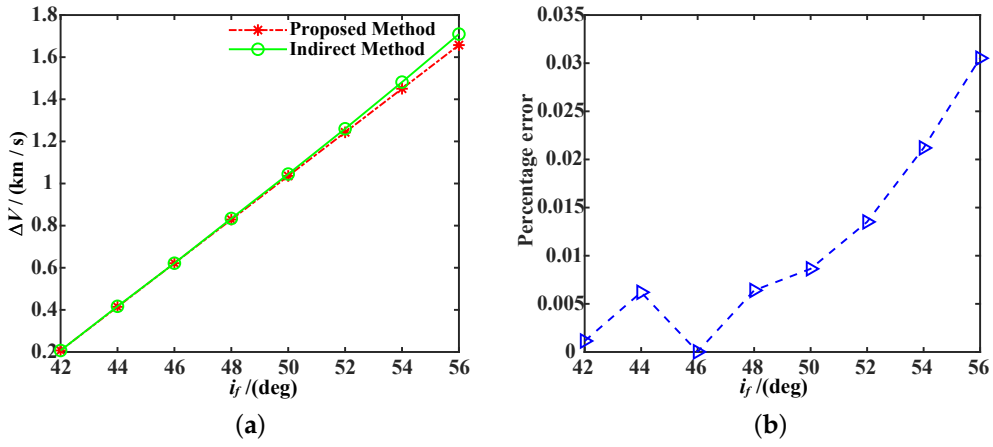


**Figure 4.** Comparison of $\Delta V$, for example 1. (**a**) $\Delta V$ solved by the two methods. (**b**) Percentage error of the estimation of $\Delta V$.

In example 2, the velocity increment estimated by the proposed method is obtained by taking the vector addition of the tangential component $\Delta V_{P,t}$ and the normal component $\Delta V_{P,h}$. First, using the proposed method in Section 3.1, we can increase the semi-major axis to its target by applying the tangent acceleration. The time of flight is calculated as

$\mathrm{ToF}_P = \sum_1^N \mathrm{ToF}_{P,k}$. The semi-major axis of the target is the stopping condition, then the flight time can be obtained by the linear interpolation as $a_{N-1} \leq a_f < a_N$

$$\mathrm{ToF}_{P,t} = \sum_{k=1}^{N-1} \mathrm{ToF}_{P,k} + \frac{a_f - a_{N-1}}{a_N - a_{N-1}} \mathrm{ToF}_{P,N} \tag{63}$$

where the $\mathrm{ToF}_{P,k}$ denotes the flight time of the $k$-th orbital revolution. The velocity increment $\Delta V_{P,t}$ can be calculated as $\Delta V_{P,t} = a_{\max} \mathrm{ToF}_{P,t}$.

Then, using the proposed method in Section 3.3, we can obtain the flight time $\Delta V_{P,h}$, by linear interpolation, as $i_{N-1} \leq i_f < i_N$

$$\mathrm{ToF}_{P,h} = \sum_{k=1}^{N-1} \mathrm{ToF}_{P,k} + \frac{i_f - i_{N-1}}{i_N - i_{N-1}} \mathrm{ToF}_{P,N} \tag{64}$$

The velocity increment $\Delta V_{P,h}$ can be calculated as $\Delta V_{P,h} = a_{\max} \mathrm{ToF}_{P,h}$. Thus, the total velocity increment is calculated as $\Delta V_P = \sqrt{\Delta V_{P,t}^2 + \Delta V_{P,h}^2}$.

In example 2, the velocity increments estimated by the two methods are shown in Figure 5a, and the percentage error of the proposed method in estimating the $\Delta V$ is shown in Figure 5b. Though, the differences of the semi-major axis and of the inclination between the target and initial orbits are equal, respectively, it shows that the velocity increment decreases with the increase in initial eccentricity. Meanwhile, when the eccentricity is smaller, the percentage error of the velocity increment estimated by the proposed method is small.

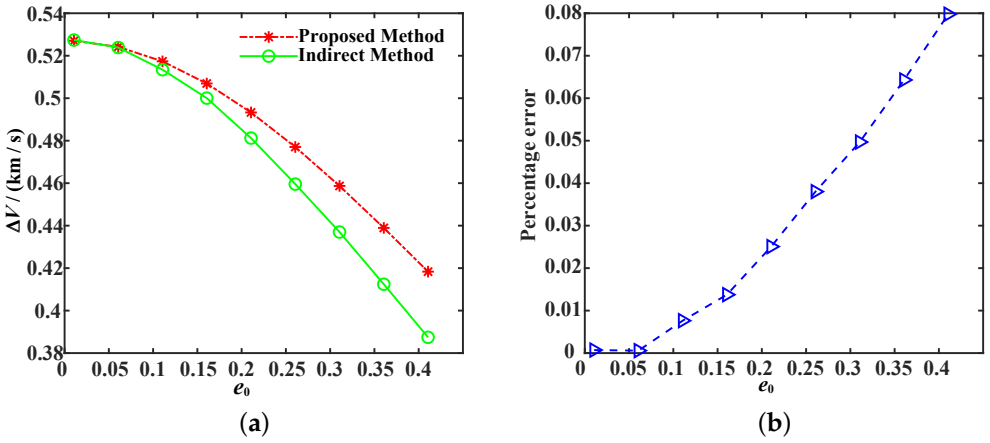


(**a**) (**b**)

**Figure 5.** Comparison of $\Delta V$ for example 2. (**a**) $\Delta V$ solved by the two methods. (**b**) Percentage error of the estimation of $\Delta V$.

Finally, the computational time of the proposed method in estimating the velocity increment of the orbital transfer is compared with the indirect method. For both of the examples, we estimate the velocity increments of eight transfers from the initial orbits to the targets. The average computational times are calculated and listed in Table 6. The proposed method takes 0.43 ms on average and 0.061 ms on average to estimate the velocity increments for a single transfer in examples 1 and 2, respectively. However, the indirect method spends tens of seconds and several seconds on average. Compared with the indirect method, the computational time of the proposed method could be reduced by over five orders of magnitude. It indicates that the proposed method has a great advantage in computational time saving in estimating the velocity increment of the orbital transfer.

**Table 6.** Computational times of two methods.

| Average Computational Time | Example 1 | Example 2 |
|---|---|---|
| Proposed method, s | $4.3 \times 10^{-4}$ | $6.1 \times 10^{-5}$ |
| Indirect method, s | 82 | 8.8 |

## 5. Discussion

The assessment of the state reachability of the low-thrust spacecraft provides a meaningful reference for the preliminary design of space missions. We conduct an efficient method for approximating the variation maxima to assess the reachability. The direct method solver, GPOPS, is used as a comparison to validate the optimality of the indirect method. It indicates that the performance of the indirect method is comparable to that of GPOPS in terms of the optimality. By solving the time-consuming numerical shooting functions, the indirect method works out the solution. Compared with the solution of the indirect method, the approximations for the secular variation maxima obtained by the proposed method are of high efficiency and accuracy. Though the indirect method gives a better solution, the proposed method reduces the computational time by over five orders of magnitude, and the percentage error is on the order of one-thousandth in general. Compared with strategy 2, strategy 1 gives a similar solution, but its computational time is reduced a lot. The accuracy and efficiency are still guaranteed, considering the $J_2$ perturbation and low-thrust acceleration. Meanwhile, the simulation results of cases 1–3 in Table 4 are consistent with the analysis of the analytical expressions. The estimation of the velocity increment for two kinds of orbital transfers is conducted and demonstrates the usefulness of the proposed method.

However, there are some limitations to this paper. We applied some simplified assumptions of the variational equations to obtain the analytical solution, such as the neglects of the mass consumption and the variation of the true anomaly caused by the low thrust. Though these assumptions are applied, the accuracy is still guaranteed. Meanwhile, the application of the proposed method in estimating the velocity increment of the orbital transfer is conducted in several special cases, such as the increment of the inclination and the semi-major axis. A further application in estimating the velocity increment for a general orbital transfer is of great significance.

## 6. Conclusions

In this paper, an approximation method is established to obtain the secular variation maxima of the classical orbital elements of low-thrust spacecraft over a finite flight time. First, the variation maxima of each orbital element over one revolution are derived analytically by applying the optimal control profile. The power series in the eccentricity are employed to expand the integrals, which have no analytical primitive functions. Then, an iterative algorithm is established to obtain the secular variation maxima of the semi-major axis, the eccentricity, and the argument of periapsis. Meanwhile, two strategies with a number of explicit expressions are conducted to approximate the secular variation maxima of the inclination and the right ascension of the ascending node. Particularly, the variation maxima of the right ascension of the ascending node and the argument of the periapsis take into account the effects of the low-thrust acceleration and of the $J_2$ perturbation of the Earth.

Two kinds of simulations are given to compare the solutions of the proposed method with the indirect method. The simulations of the variation maximum of each orbital element are conducted and demonstrate the efficiency and accuracy of the proposed method. In general, the percentage errors in approximating the variational maxima are on the order of one thousandth. Meanwhile, a preliminary application of the approximation of the secular variation maxima is given to estimate the velocity increments of low-thrust orbital transfers. The simulation demonstrates that the proposed method has a high estimating accuracy compared with the indirect method. The percentage error is on the order of one percent. In particular, both kinds of simulations indicate that the computational times of

the proposed method are reduced by over five orders of magnitude, as compared with the indirect method.

## 7. Future Work

In this paper, we have demonstrated an efficient method with analytical derivations to approximate the secular maxima of the classical orbital elements and the preliminary application of the proposed method. It is foreseeable that the fast and accurate estimate of the variation maxima of the orbital elements can provide a priori information for the low-thrust trajectory design and optimization. Thus, the proposed method can bring benefits to the sequence search of multi-target low-thrust missions. Meanwhile, given the limitations of this paper, it will be important that future research investigates the variation maxima of the orbital elements, considering the mass consumption. Additionally, a significant topic for future research might be the estimation of the velocity increment for a general orbital transfer, taking into account the combination of various orbital elements.

**Author Contributions:** Z.W. and L.C. completed the preliminary research and provided the numerical part; Z.W. and F.J. conceived and wrote the paper; F.J. supervised the overall work and reviewed the paper. All authors have read and agreed to the published version of the manuscript.

**Funding:** This work was supported by the National Natural Science Foundation of China (No. 12022214).

**Institutional Review Board Statement:** Not applicable.

**Informed Consent Statement:** Not applicable.

**Data Availability Statement:** The data presented in this study are available on request from the corresponding author.

**Conflicts of Interest:** The authors declare no conflict of interest.

## Nomenclature

| Symbols | |
|---|---|
| $a$ | Semi-major axis |
| $e$ | Eccentricity |
| $i$ | Inclination |
| $\Omega$ | Right ascension of ascending node |
| $\omega$ | Argument of periapsis |
| $f$ | True anomaly |
| $h$ | Magnitude of specific angular momentum |
| $\mu$ | Gravitational constant |
| $\boldsymbol{a}$ | Propulsive acceleration vector |
| $\Delta\boldsymbol{x}$ | Variation group of the classical orbital elements over one orbital revolution |
| $\boldsymbol{x}_N$ | Values of the orbital elements after $N$ orbital revolutions |
| $T_{\max}$ | Thrust magnitude |
| $R_E$ | Mean equatorial radius of the Earth |
| $J_2$ | Second order zonal harmonic of the Earth's gravitational potential |
| $\Delta V$ | Velocity increment |
| $\boldsymbol{X}$ | Group of the orbital elements |
| $\boldsymbol{u}$ | Thrust vector |
| $u$ | Engine thrust ratio |
| $\boldsymbol{\alpha}$ | Unit vector of thrust direction |
| ToF | Time of flight |
| $\boldsymbol{\lambda}$ | Lagrange multiplier associated with state, i.e., costate |
| $H$ | Hamiltonian |
| AU | Astronomical unit |
| $\boldsymbol{\Phi}$ | Combination of shooting functions |
| $m$ | Instantaneous mass of spacecraft |
| $\beta$ | Out-of-plane (yaw) steering angle |
| $\alpha$ | In-plane thrust-steering angle |

| Subscripts | |
|---|---|
| $LT$ | Low thrust |
| $J_2$ | $J_2$ perturbation |
| $P$ | Proposed method |
| $I$ | Indirect method |
| $N$ | $N$-th orbital revolution |
| 0 | Initial time |
| $f$ | Final time |

## References


1. Rayman, M.D.; Williams, S.N. Design of the first interplanetary solar electric propulsion mission. *J. Spacecr. Rocket.* **2002**, *39*, 589–595. [CrossRef]
2. Benkhoff, J.; Van Casteren, J.; Hayakawa, H.; Fujimoto, M.; Laakso, H.; Novara, M.; Ferri, P.; Middleton, H.R.; Ziethe, R. BepiColombo—Comprehensive exploration of Mercury: Mission overview and science goals. *Planet. Space Sci.* **2010**, *58*, 2–20. [CrossRef]
3. Alemany, K.; Braun, R. Survey of Global Optimization Methods for Low-Thrust, Multiple Asteroid Tour Missions. In Proceedings of the AAS/AIAA Space Flight Mechanics Meeting, Sedona, AZ, USA, 28 January–1 February 2007.
4. Morante, D.; Sanjurjo Rivo, M.; Soler, M. A Survey on Low-Thrust Trajectory Optimization Approaches. *Aerospace* **2021**, *8*, 88. [CrossRef]
5. Chen, Y.; Baoyin, H.; Li, J. Accessibility of main-belt asteroids via gravity assists. *J. Guid. Control Dyn.* **2014**, *37*, 623–632. [CrossRef]
6. Liu, E.; Yan, Y.; Yang, Y. Analysis and determination of capture area for space debris removal based on reachable domain. *Adv. Space Res.* **2021**, *68*, 1613–1626. [CrossRef]
7. Dahl, J.; de Campos, G.R.; Olsson, C.; Fredriksson, J. Collision avoidance: A literature review on threat-assessment techniques. *IEEE Trans. Intell. Veh.* **2018**, *4*, 101–113. [CrossRef]
8. Holzinger, M.; Scheeres, D. Applied reachability for space situational awareness and safety in spacecraft proximity operations. In Proceedings of the AIAA Guidance, Navigation, and Control Conference, Chicago, IL, USA, 10–13 August 2009; p. 6096.
9. Xu, Z.; Chen, X.; Huang, Y.; Bai, Y.; Chen, Q. Collision prediction and avoidance for satellite ultra-close relative motion with zonotope-based reachable sets. *Proc. Inst. Mech. Eng. Part G J. Aerosp. Eng.* **2019**, *233*, 3920–3937. [CrossRef]
10. Lee, S.; Hwang, I. Reachable set computation for spacecraft relative motion with energy-limited low-thrust. *Aerosp. Sci. Technol.* **2018**, *77*, 180–188. [CrossRef]
11. Battin, R.H. *An Introduction to the Mathematics and Methods of Astrodynamics*, Revised Edition; American Institute of Aeronautics and Astronautics: Reston, VA, USA, 1999.
12. Xue, D.; Li, J.; Baoyin, H.; Jiang, F. Reachable Domain for Spacecraft with a Single Impulse. *J. Guid. Control Dyn.* **2010**, *33*, 934–942. [CrossRef]
13. Li, X.H.; He, X.S.; Zhong, Q.F. Investigation on Reachable Domain of Satellite with a Single Impulse. *Adv. Mater. Res.* **2012**, *433–440*, 5759–5766. [CrossRef]
14. Wen, C.; Peng, C.; Gao, Y. Reachable domain for spacecraft with ellipsoidal Delta-V distribution. *Astrodynamics* **2018**, *2*, 265–288. [CrossRef]
15. Vinh, N.X.; Gilbert, E.G.; Howe, R.M.; Sheu, D.; Lu, P. Reachable domain for interception at hyperbolic speeds. *Acta Astronaut.* **1995**, *35*, 1–8. [CrossRef]
16. Zhang, G.; Cao, X.; Ma, G. Reachable domain of spacecraft with a single tangent impulse considering trajectory safety. *Acta Astronaut.* **2013**, *91*, 228–236. [CrossRef]
17. Zhang, J.; Yuan, J.; Wang, W.; Wang, J. Reachable domain of spacecraft with a single normal impulse. *Aircr. Eng. Aerosp. Technol.* **2019**, *91*, 977–986. [CrossRef]
18. Li, X.; He, X.; Zhong, Q.; Song, M. Reachable domain for satellite with two kinds of thrust. *Acta Astronaut.* **2011**, *68*, 1860–1864. [CrossRef]
19. Betts, J.T. Survey of Numerical Methods for Trajectory Optimization. *J. Guid. Control Dyn.* **1998**, *21*, 193–207. [CrossRef]
20. Russell, R.P. Primer vector theory applied to global low-thrust trade studies. *J. Guid. Control Dyn.* **2007**, *30*, 460–472. [CrossRef]
21. Li, X.; Qiao, D.; Chen, H. Interplanetary transfer optimization using cost function with variable coefficients. *Astrodynamics* **2019**, *3*, 173–188. [CrossRef]
22. Liu, X.; Lu, P.; Pan, B. Survey of convex optimization for aerospace applications. *Astrodynamics* **2017**, *1*, 23–40. [CrossRef]
23. Vasile, M.; Minisci, E.; Locatelli, M. Analysis of some global optimization algorithms for space trajectory design. *J. Spacecr. Rocket.* **2010**, *47*, 334–344. [CrossRef]
24. Topputo, F.; Zhang, C. Survey of Direct Transcription for Low-Thrust Space Trajectory Optimization with Applications. *Abstr. Appl. Anal.* **2014**, *2014*, 1–15. [CrossRef]
25. Tang, G.; Jiang, F.; Li, J. Low-thrust trajectory optimization of asteroid sample return mission with multiple revolutions and moon gravity assists. *Sci. China Phys. Mech. Astron.* **2015**, *58*, 114501. [CrossRef]

26. Hudson, J.S.; Scheeres, D.J. Orbital targeting using reduced eccentric anomaly low-thrust coefficients. *J. Guid. Control Dyn.* **2011**, *34*, 820–831. [CrossRef]
27. Ko, H.C.; Scheeres, D.J. Essential thrust-Fourier-coefficient set of averaged Gauss equations for orbital mechanics. *J. Guid. Control Dyn.* **2014**, *37*, 1236–1249. [CrossRef]
28. Caruso, A.; Bassetto, M.; Mengali, G.; Quarta, A.A. Optimal solar sail trajectory approximation with finite Fourier series. *Adv. Space Res.* **2021**, *67*, 2834–2843. [CrossRef]
29. Taheri, E.; Abdelkhalik, O. Initial three-dimensional low-thrust trajectory design. *Adv. Space Res.* **2016**, *57*, 889–903. [CrossRef]
30. Huo, M.; Zhang, G.; Qi, N.; Liu, Y.; Shi, X. Initial trajectory design of electric solar wind sail based on finite Fourier series shape-based method. *IEEE Trans. Aerosp. Electron. Syst.* **2019**, *55*, 3674–3683. [CrossRef]
31. Zhang, T.; Wu, D.; Jiang, F.; Zhou, H. A New 3D Shaping Method for Low-Thrust Trajectories between Non-Intersect Orbits. *Aerospace* **2021**, *8*, 315. [CrossRef]
32. Nie, T.; Gurfil, P. Long-term evolution of orbital inclination due to third-body inclination. *Celest. Mech. Dyn. Astron.* **2021**, *133*, 1–33. [CrossRef]
33. Colombo, C.; Vasile, M.; Radice, G. Semi-Analytical Solution for the Optimal Low-Thrust Deflection of Near-Earth Objects. *J. Guid. Control Dyn.* **2009**, *32*, 796–809. [CrossRef]
34. Gao, Y.; Kluever, C. Analytic orbital averaging technique for computing tangential-thrust trajectories. *J. Guid. Control Dyn.* **2005**, *28*, 1320–1323. [CrossRef]
35. Gonzalo, J.L.; Bombardelli, C. Multiple scales asymptotic solution for the constant radial thrust problem. *Celest. Mech. Dyn. Astron.* **2019**, *131*, 37. [CrossRef]
36. Carlo, M.D.; da Graça Marto, S.; Vasile, M. Extended analytical formulae for the perturbed Keplerian motion under low-thrust acceleration and orbital perturbations. *Celest. Mech. Dyn. Astron.* **2021**, *133*, 13. [CrossRef]
37. Izzo, D.; Märtens, M.; Pan, B. A survey on artificial intelligence trends in spacecraft guidance dynamics and control. *Astrodynamics* **2019**, *3*, 287–299. [CrossRef]
38. Tsukamoto, H.; Chung, S.J.; Slotine, J.J. Learning-based Adaptive Control via Contraction Theory. *arXiv* **2021**, arXiv:2103.02987.
39. Gaudet, B.; Linares, R.; Furfaro, R. Deep reinforcement learning for six degree-of-freedom planetary landing. *Adv. Space Res.* **2020**, *65*, 1723–1741. [CrossRef]
40. Gao, Y.; Kluever, C. Engine-switching strategies for interplanetary solar-electric-propulsion spacecraft. *J. Spacecr. Rocket.* **2005**, *42*, 765–767. [CrossRef]
41. Henninger, H.C.; Biggs, J.D. Near time-minimal Earth to L1 transfers for low-thrust spacecraft. *J. Guid. Control Dyn.* **2017**, *40*, 2999–3004. [CrossRef]
42. Abramowitz, M.; Stegun, I.A. *Handbook of Mathematical Functions with Formulas, Graphs, and Mathematical Tables*; US Government Printing Office: Washington, DC, USA, 1964; Volume 55.
43. Kluever, C.A. Simple guidance scheme for low-thrust orbit transfers. *J. Guid. Control Dyn.* **1998**, *21*, 1015–1017. [CrossRef]
44. Petropoulos, A.E. *Simple Control Laws for Low-Thrust Orbit Transfers*; Jet Propulsion Laboratory, National Aeronautics and Space Administration: Pasadena, CA, USA, 2003.
45. Bassetto, M.; Quarta, A.A.; Mengali, G. Locally-optimal electric sail transfer. *Proc. Inst. Mech. Eng. Part G J. Aerosp. Eng.* **2019**, *233*, 166–179. [CrossRef]
46. Vallado, D.A. *Fundamentals of Astrodynamics and Applications*; Springer Science & Business Media: Berlin/Heidelberg, Germany, 2001; Volume 12.
47. Sidi, M.J. *Spacecraft Dynamics and Control: A Practical Engineering Approach*; Cambridge University Press: Cambridge, UK, 1997; Volume 7.
48. Rao, A.V.; Benson, D.A.; Darby, C.; Patterson, M.A.; Francolin, C.; Sanders, I.; Huntington, G.T. Algorithm 902: Gpops, a matlab software for solving multiple-phase optimal control problems using the gauss pseudospectral method. *ACM Trans. Math. Softw. (TOMS)* **2010**, *37*, 1–39. [CrossRef]
49. Jiang, F.; Baoyin, H.; Li, J. Practical Techniques for Low-Thrust Trajectory Optimization with Homotopic Approach. *J. Guid. Control Dyn.* **2012**, *35*, 245–258. [CrossRef]
50. Hull, D.G. *Optimal Control Theory for Applications*; Springer Science & Business Media: Berlin/Heidelberg, Germany, 2013.
51. Moré, J.J.; Garbow, B.S.; Hillstrom, K.E. *User Guide for MINPACK-1*; Argonne National Laboratory: Argonne, IL, USA, 1980; ANL-80-74.